Supplementary Information

Constructing a quasi-liquid interphase to enable highly stable Zn-metal anode

Junzhang Wang[a], Zhou Xu[a], Tengteng Qin[a], Jintian Wang[a], Rui Tian[a], Xingzhong Guo[a,b], Zongrong Wang[a], Zhongkuan Luo[c], Hui Yang[a, b]*

[a] State Key Laboratory of Silicon and Advanced Semiconductor Materials, School of Materials Science and Engineering, Zhejiang University, Hangzhou 310058, China.

[b] Hangzhou Global Scientific and Technological Innovation Center, Zhejiang University, Hangzhou 311200, China.

[c] Zhejiang-California International Nanosystems Institute, Zhejiang University, Hangzhou 310058, China.

*Corresponding E-mail: msewj01@zju.edu.cn

1. Simulation details

The 2D numerical model was calculated by the module "Tertiary Current Distribution, Nernst-Planck" of COMSOL software. The diffusion coefficient of Zn^{2+} in the electrolyte of 2 M $ZnSO_4$ was set to 2×10^{-9} m^2 s^{-1}. The cathode was set as the upper boundary of the 50 μm electrolyte. A coating with 5 μm thickness was on the anode surface, where the gap was filled with 0.25 μm electrolyte. The diffusion coefficient of Zn^{2+} in the coatings was set to 2×10^{-10} m^2 s^{-1}.

To create non-uniformity in the coating, the diffusion coefficient of Zn^{2+} in the coating was spatially modified according the Gaussian function as follows: [1]

$$g1(x) = \exp\left(\frac{-x^2}{2\sigma^2}\right) \qquad \text{(Equation S1)}$$

$$\sigma = \frac{5\times10^{-6}m}{2\sqrt{2\ln 2}} \qquad \text{(Equation S2)}$$

Where the full-width half-maximum of the coating was 5 μm, and the maximum amplitude at the center is 2×10^{-9} m^2 s^{-1}. To give the coating a self-adaptive dynamic behavior, a feedback mechanism was added to the spatially varying Gaussian conductivity profile. The Gaussian distribution was attenuated by a factor of $e^{-A\Delta V}$, where A is a scaling factor and ΔV is the volume change of each mesh element in the coating with Zn metal deposition. The overpotential was set to -135 mV (vs. Zn/Zn^{2+}) at the Zn anode.

For comparison, the same parameters were used for electrodes with a SSI. Moreover, we introduced ellipses (long diameter 2.5 μm, short diameter 1.25 μm) filled with electrolyte or air. For the rigid SSI, a 5 μm pinhole was introduced to generate non-uniformity as a control. For the anode without coating, the initial bumps were introduced since the dendrite growth mainly depends on the surface roughness. This is a typical dendritic evolution problem, where the Bulter-Volmer current density i_{BV} is regulated by a rate modification factor S [2].

2. Supporting Figures

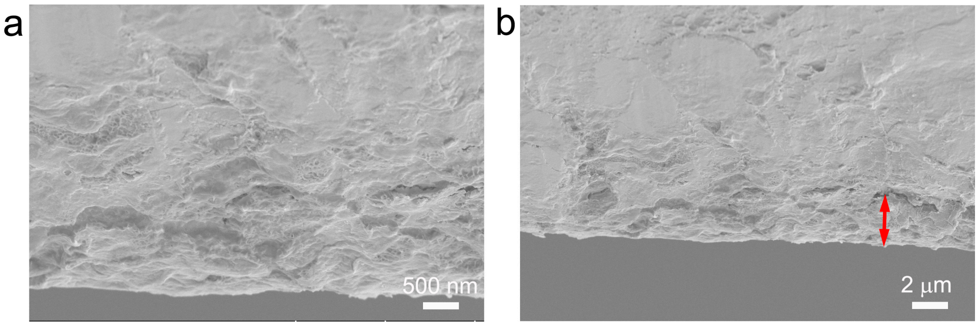

Figure S1. SEM images of Zn@QLI in the cross-section direction, indicating the thickness of the modifed layer is ~3 μm.

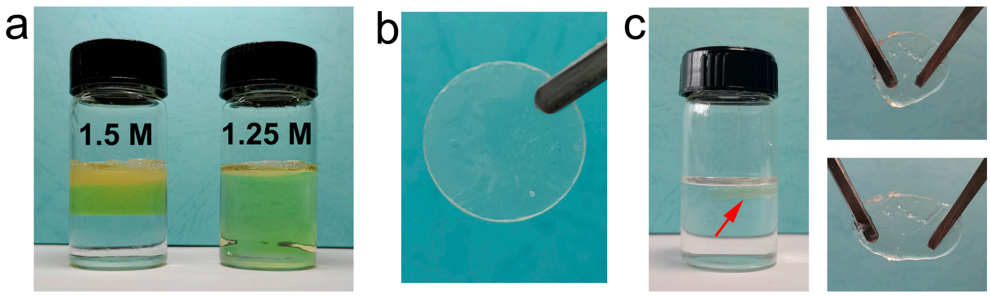

Figure S2. The gelatin solutions with 1.5 or 1.25 M $ZnSO_4$ solutions. The modified layer before (b) and after immersing (c) in 2 M $ZnSO_4$ solution.

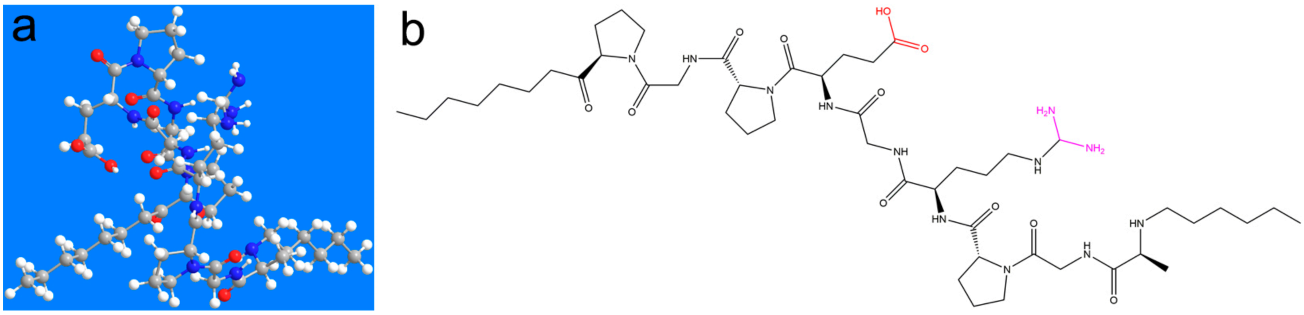

Figure S3. (a) 3D and (b) 2D models of one of the gelatin molecules [3].

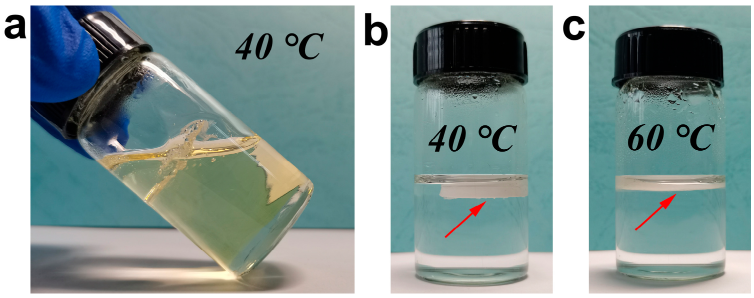

Figure S4. (a) The solid gelatin electrolyte at 40 °C. The Gel that immersed in 2 M $ZnSO_4$ electrolyte at 40 °C (b) and 60 °C (c).

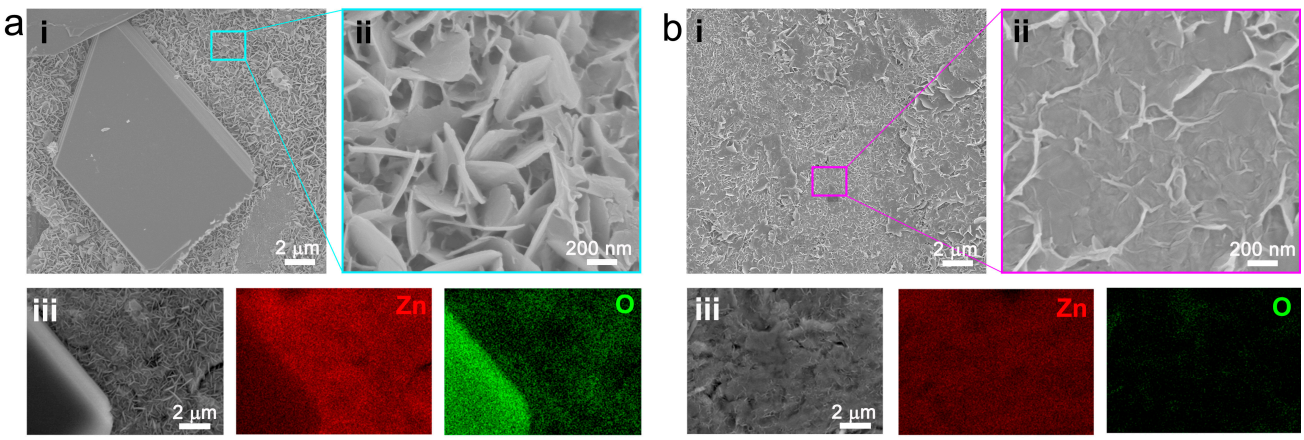

Figure S5. SEM images and corresponding EDS mappings after immersing Zn (a) and Zn@QLI (b) into 2 M $ZnSO_4$ electrolyte for 8 days.

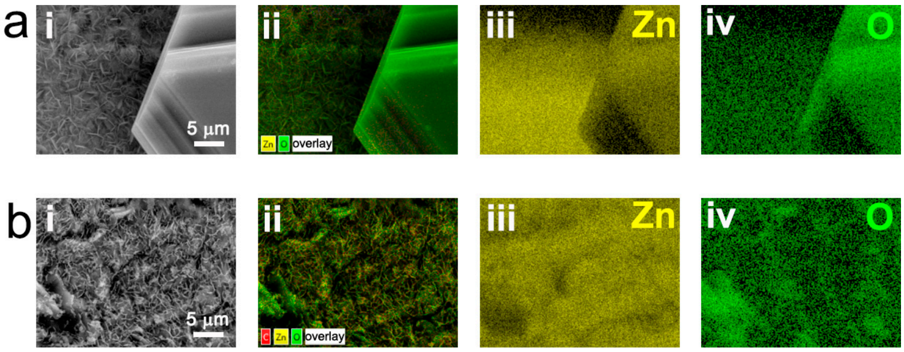

Figure S6. The EDS mappings after immersing Zn (a) and Zn@QLI (b) into 2 M $ZnSO_4$ electrolyte for 16 days.

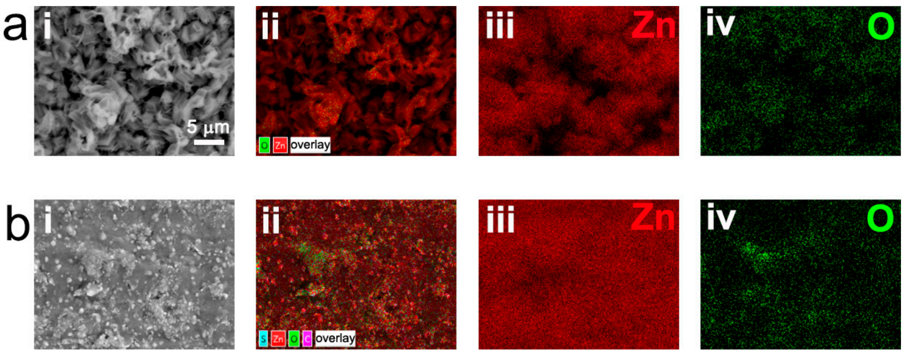

Figure S7. The EDS mappings of the surfaces after CA test for Zn (a) and Zn@QLI (b).

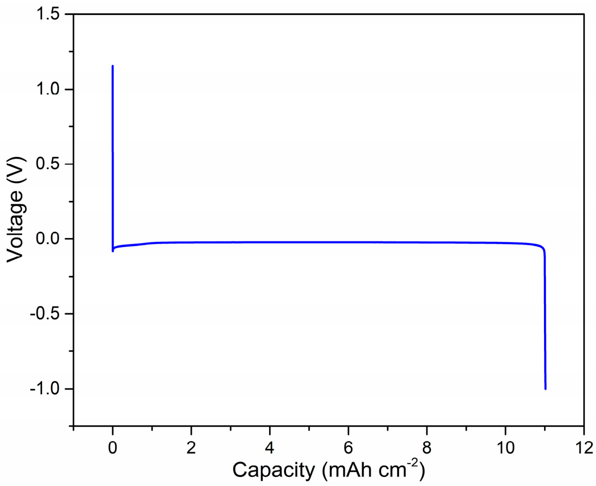

Figure S8. The discharge curve of Cu-Zn half cell, indicating the capacity of 20 μm Zn foil is ~11 mAh cm^{-2}.

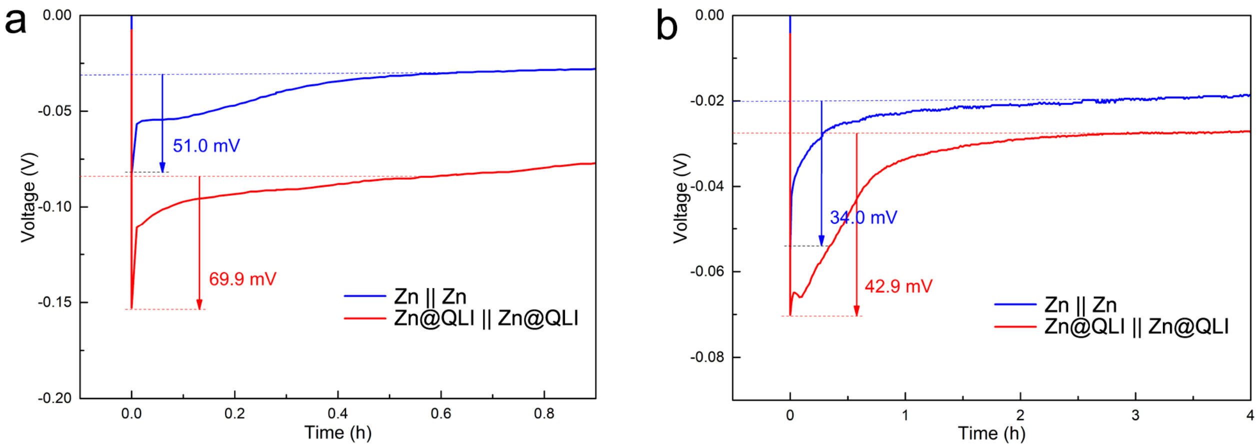

Figure S9. The nucleation overpotentials of Zn and Zn@QLI at a current density of 1 mA cm^{-2} (a) and 0.2 mA cm^{-2} (b).

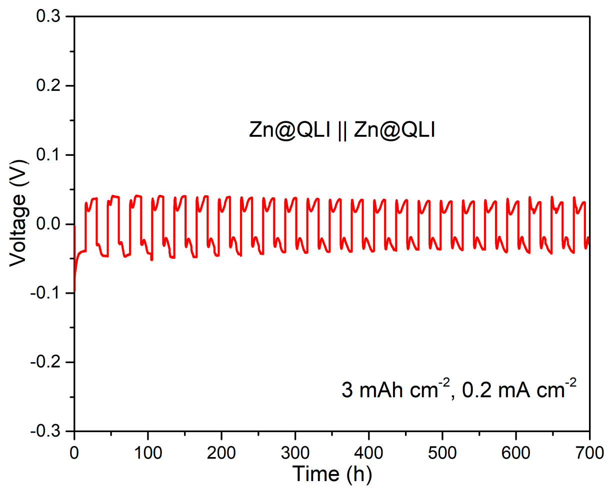

Figure S10. Galvanostatic cycling of the symmetric cell with Zn@QLI with a capacity of 3 mAh cm^{-2} at 0.2 mA cm^{-2}.

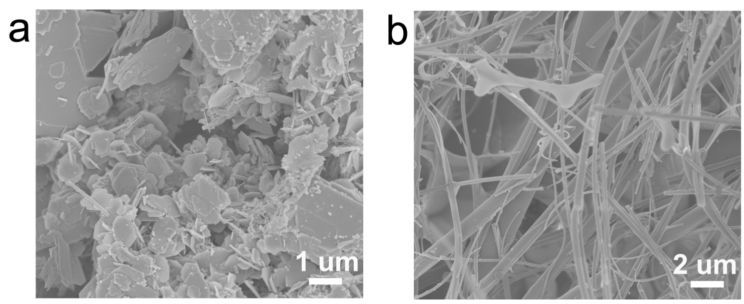

Figure S11. SEM images of the Zn (a) and Zn@QLI electrode (b) in the stripped state, after cycling for 100 h with a capacity of 1 mAh cm^{-2} at 0.2 mA cm^{-2}.

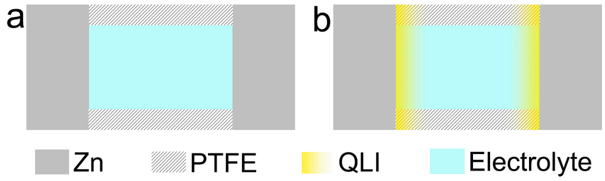

Figure S12. The cell configurations of the symmetric cell without separators for Zn (a) and Zn@QLI electrode (b).

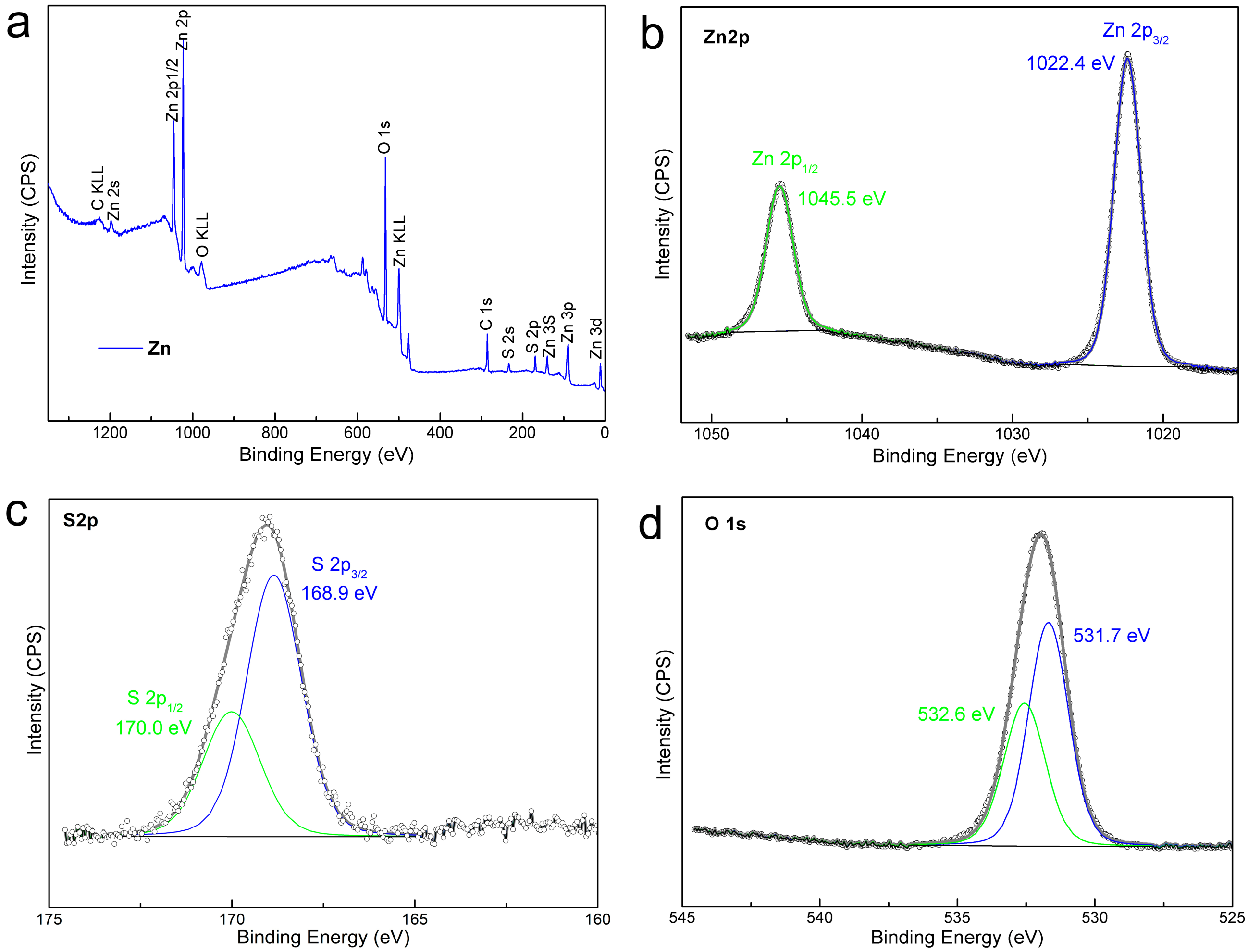

Figure S13. (a) XPS survey spectra of the bare Zn electrode after 30 h cycles with the symmetric cells without separators. The corresponding Zn 2p spectrum (b), S 2p spectrum (c) and O 1s spectrum (d).

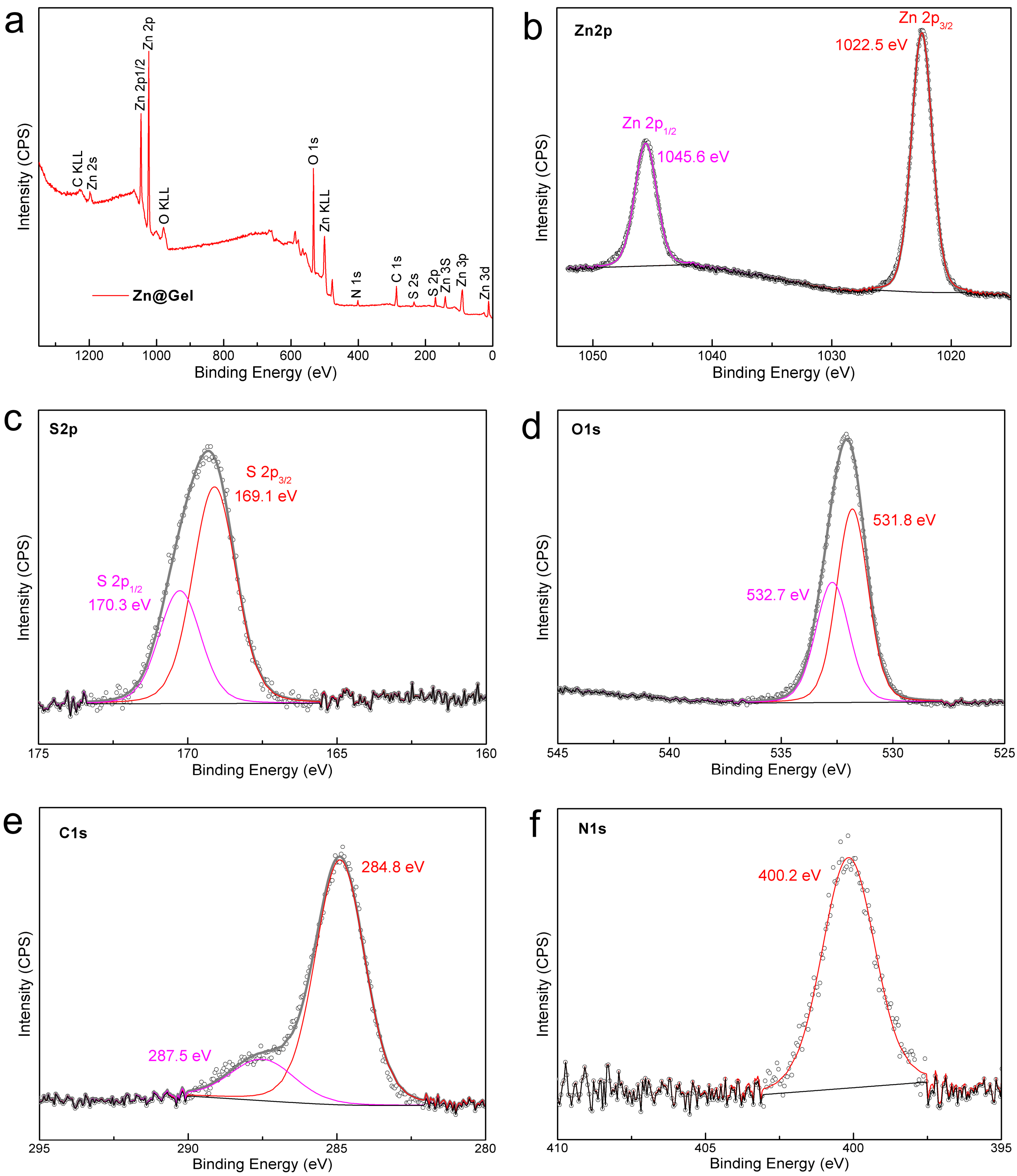

Figure S14. (a) XPS survey spectra of the Zn@QLI electrode after 30 h cycles with the symmetric cells without separators. The corresponding Zn 2p spectrum (b), S 2p spectrum (c), O 1s spectrum (d), C1s spectrum (e) and N1s spectrum (f).

The XPS survey spectra of both the Zn (Figure S13a) and the Zn@QLI electrode (Figure S14a) confirm the composition of element Zn, S and O. Figure S13b-c show the Zn 2p, S 2p and O 1s spectra of the cycled Zn electrode. The 2p orbital is split into two distinct peaks at 1022.4 and 1045.5 eV, corresponding to the $2p_{3/2}$ and $2p_{1/2}$ of Zn^{2+}, respectively. The S 2p peaks at 168.9 and 170.0 eV are assigned to multiplet-split $2p_{3/2}$ and $2p_{1/2}$ of sulfate species, which is consistent with the result of XRD. The O 1s peaks at 531.7 and 532.6 eV represent two oxygen environments in sulfate species. As shown in Figure S14b-d, the cycled Zn@QLI exhibits similar Zn 2p, S 2p and O 1s spectra compared to the Zn electrode. Although the QLI has been removed, a new C 1s peak at 287.5 eV and a new N 1s peak at 400.2 eV appear (Figure S14e and f), which can be attributed to the residual of the QLI.

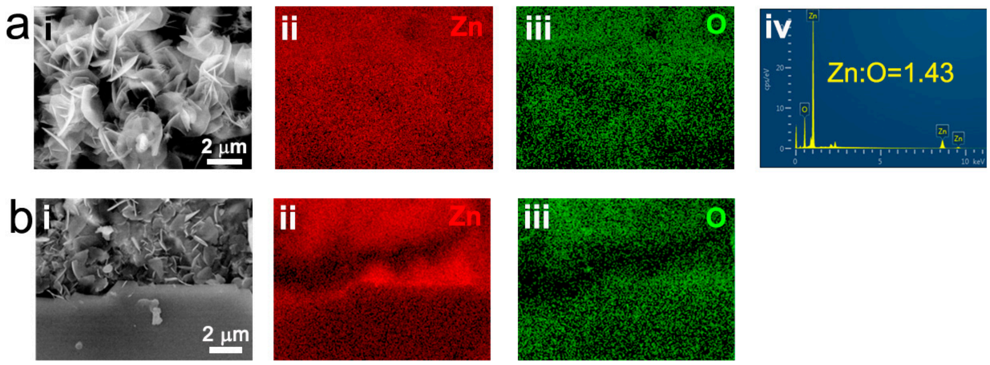

Figure S15. EDS mappings of the Zn electrode in the symmetric cell without separators after 30 h cycles. The particle (a) and flat area (b) corresponding to Figure 4c.

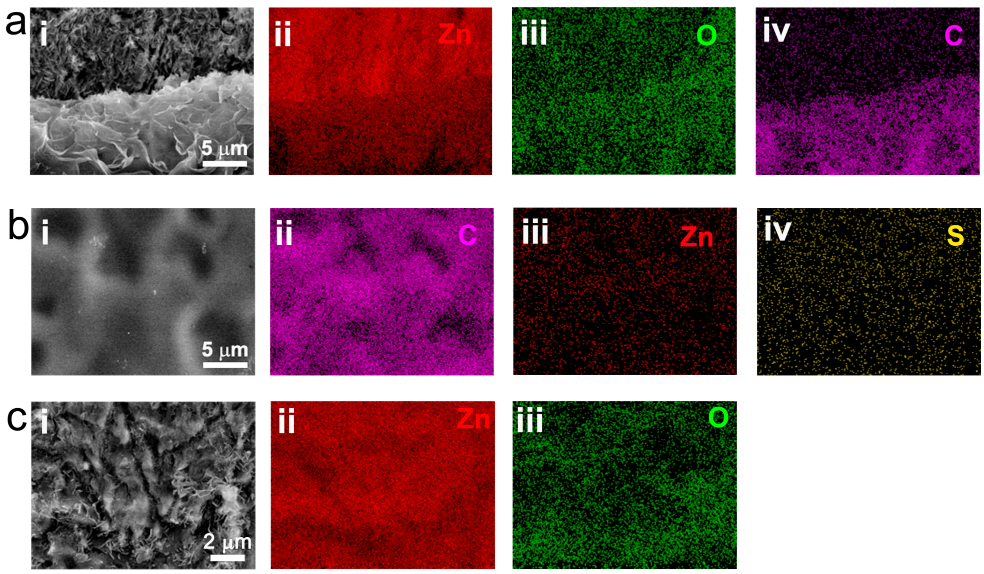

Figure S16. EDS mappings of the Zn@QLI electrode in the symmetric cell without separators after

30 h cycles. The QLI edge (a), QLI (b) and the area under QLI (c) corresponding to Figure 4d.

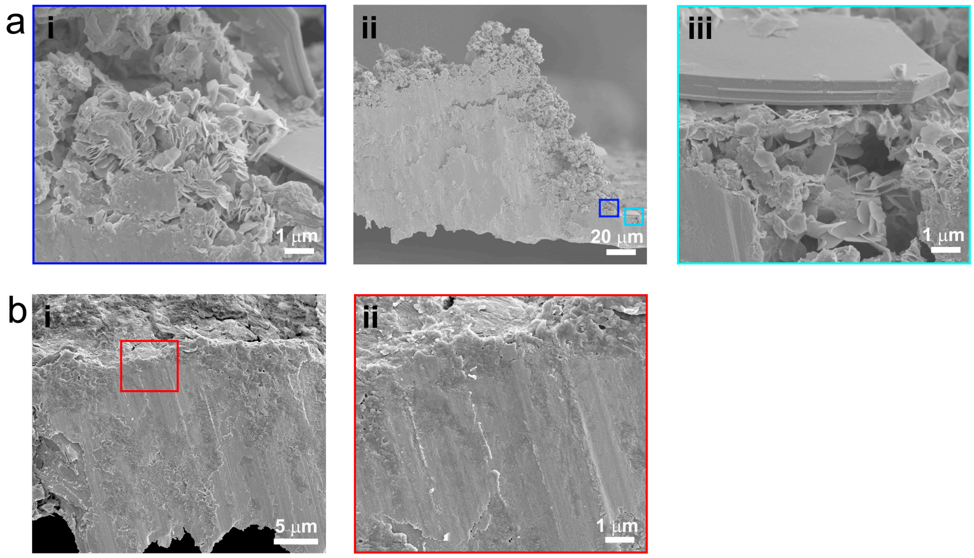

Figure S17. SEM images of Zn (a) and Zn@QLI electrode (b) after cycles in the cross-section view.

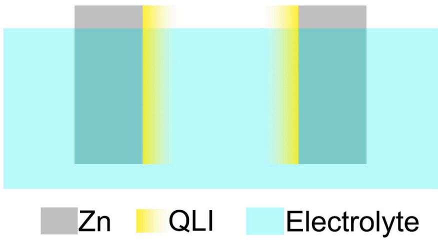

Figure S18. The cell configurations of the symmetric cell with suspended Zn@QLI electrodes.

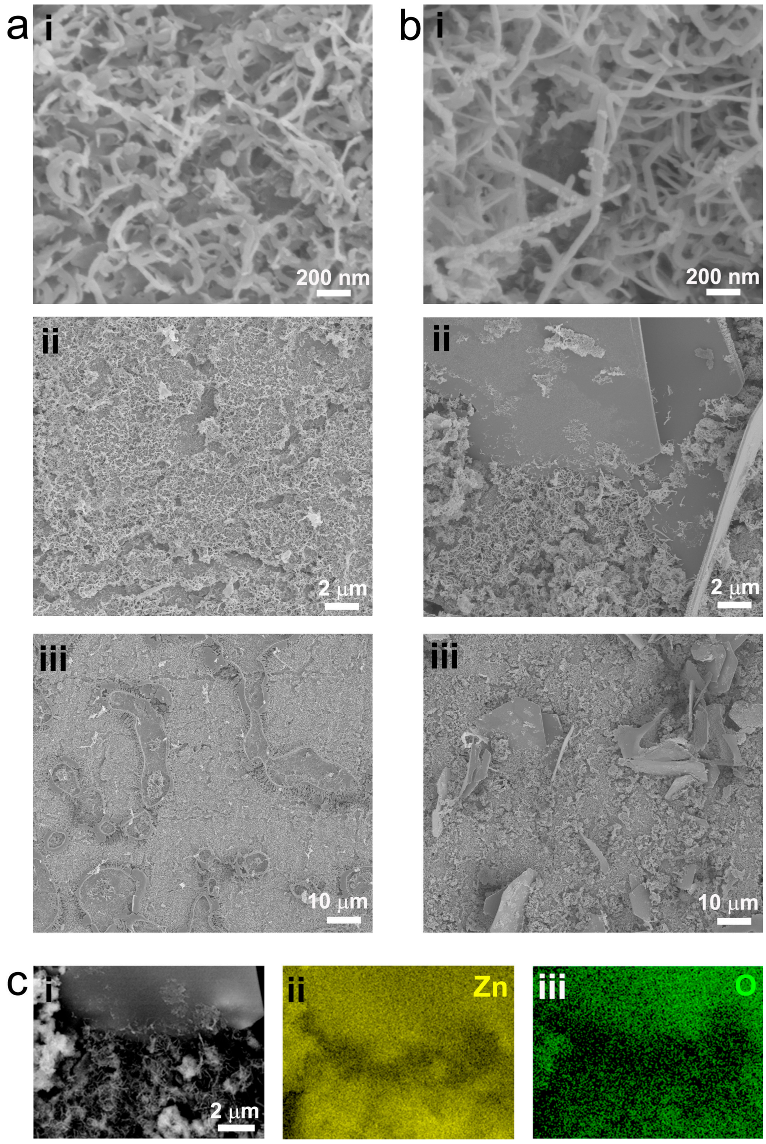

Figure S19. SEM images of the cycled bare Zn after 30 h in the plated state (a) and stripped state (b). (c) The corresponding EDS mappings in b.

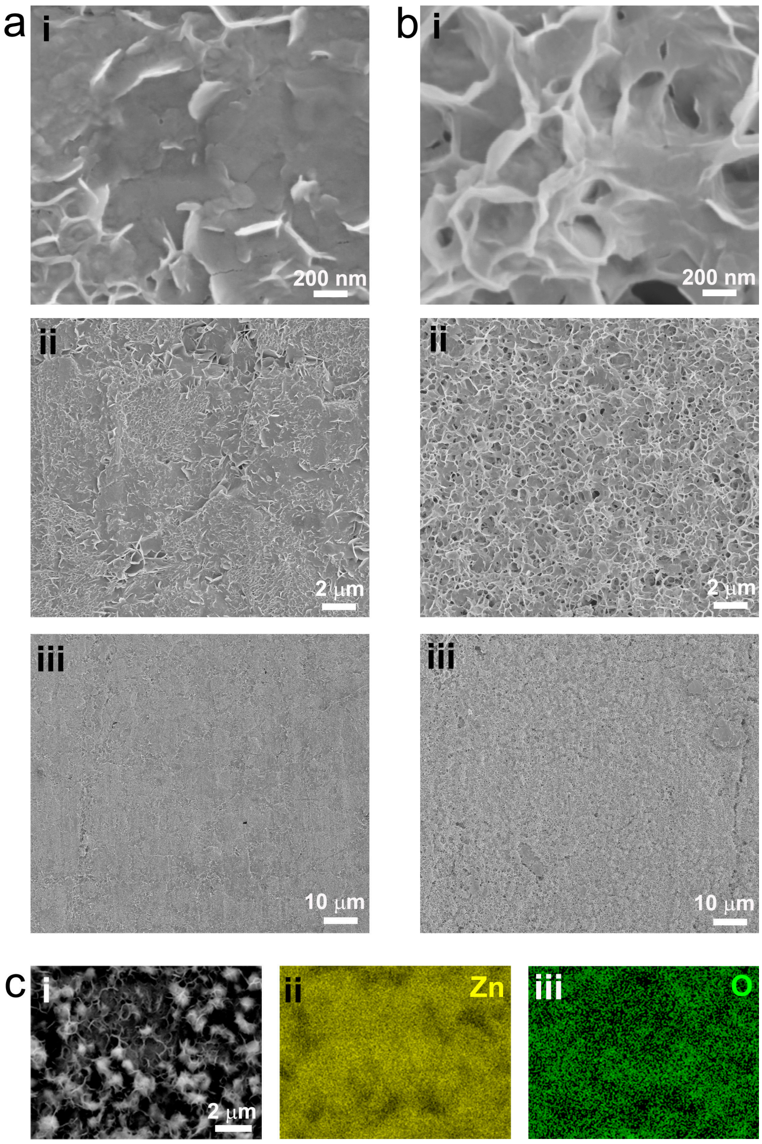

Figure S20. SEM images of the cycled Zn@QLI anode after 30 h in the plated state (a) and stripped state (b). (c) The corresponding EDS mappings in b.

Figure S19a and b show the SEM images of the cycled Zn electrode after 30 h in the plated and stripped state, respectively. The surface is composed of lots of whiskers in the plated state, while some large bulks appeared in the above non-separator symmetric cell present. The bulks are assigned to zinc oxides according to the element mapping (Figure S19c). In sharp contrast, the surface of the as-deposited Zn@QLI electrode is still flat with some winkle (Figure S20a), which is very similar to the morphology obtained from the non-separator symmetric cell. In the stripped state, the surface is rougher than that in the plated state, but still no large bulks and the distribution of element Zn and O is uniform (Figure S20b and c).

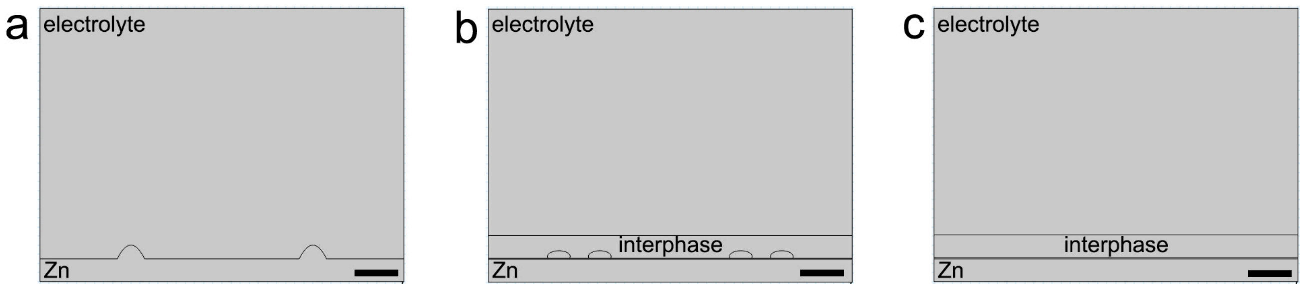

Figure S21. The simulation cell geometry in COMSOL for the bare Zn anode (a), Zn@elastic-SSI with electrolyte filling in the oval gap (b) and Zn@QLI (c). Scale bar: 10 µm.

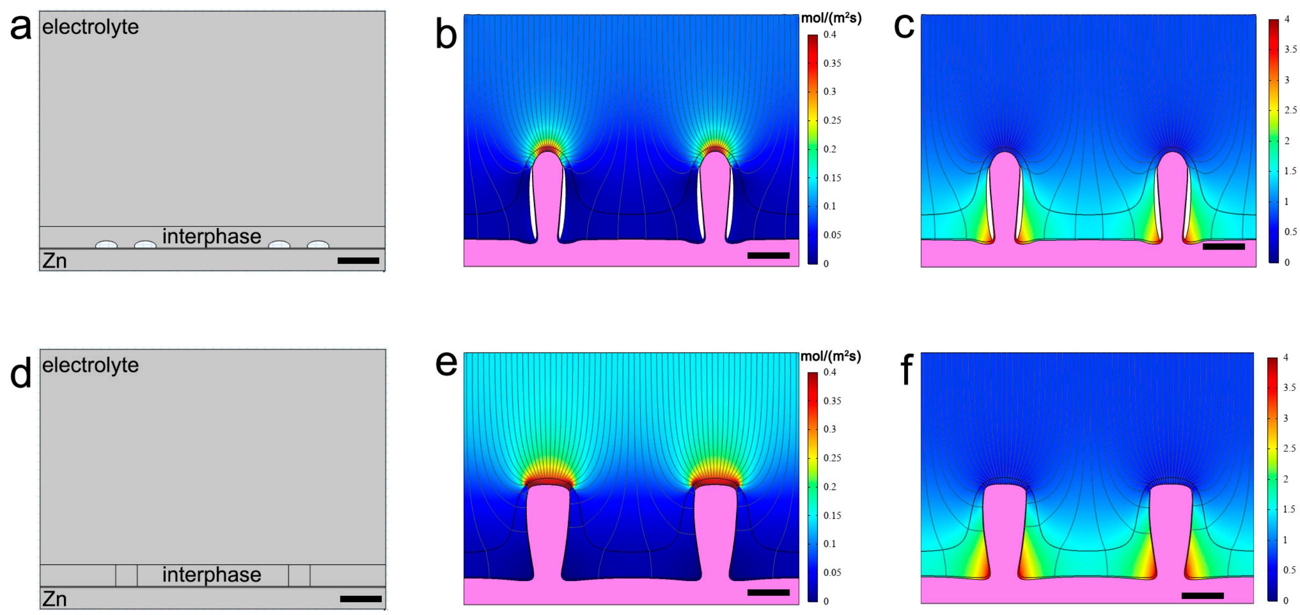

Figure S22. The simulation cell geometry in COMSOL for Zn@elatic-SSI with air filling in the oval gap (a) and Zn@rigid-SSI (d). Simulations of Zn deposition on Zn@elatic-SSI with air filling in the oval gap (b) and Zn@rigid-SSI (e). The color indicates the magnitude of spatial Zn^{2+} flux. Mesh element volume change during Zn deposition on Zn@elatic-SSI with air filling in the oval gap (c) and Zn@rigid-SSI (f). The color indicates the degree of volume change. In each snapshot, the streamlines display the direction of Zn^{2+} flux and the electrode is painted pink. Scale bar: 10 µm.

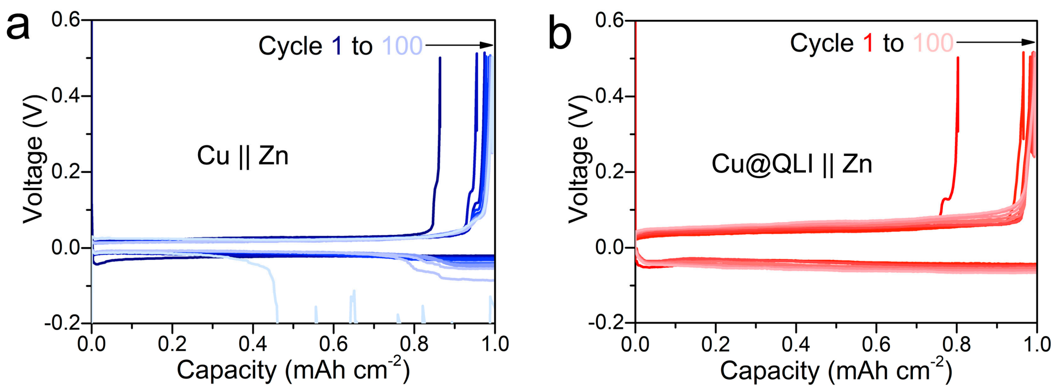

Figure S23. Voltage profiles of the Cu-Zn (a) and Cu@QLI-Zn half cell (b) with a capacity of 1 mAh cm^{-2} at 1 mA cm^{-2}.

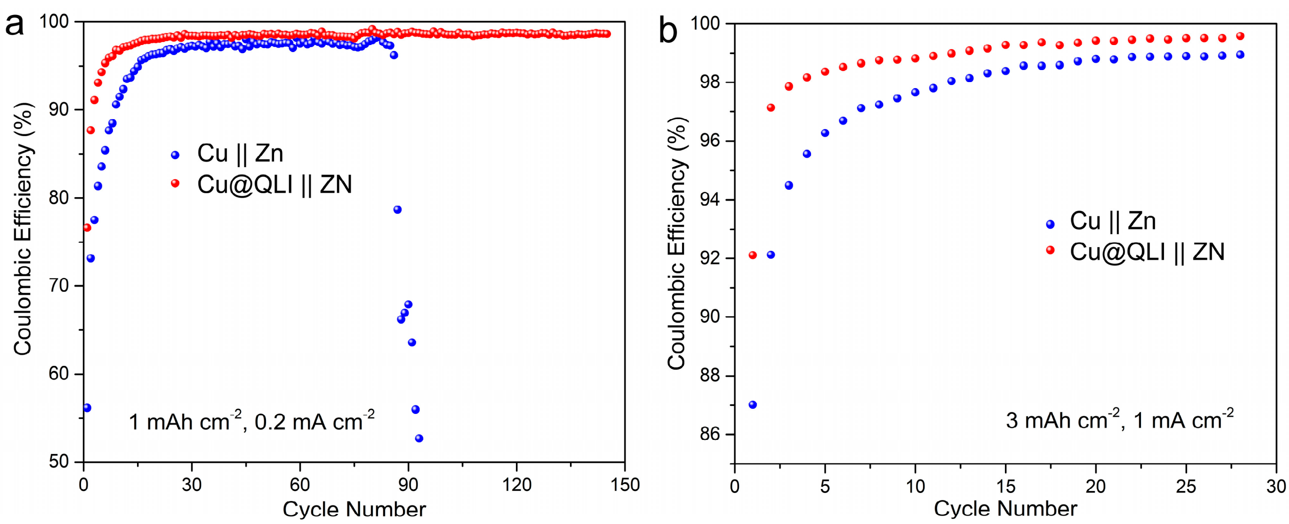

Figure S24. Coulombic efficiency of the half cells with a capacity of 1 mAh cm^{-2} at 0.2 mA g^{-1} (a) and 3 mAh cm^{-2} at 1 mA g^{-1} (b).

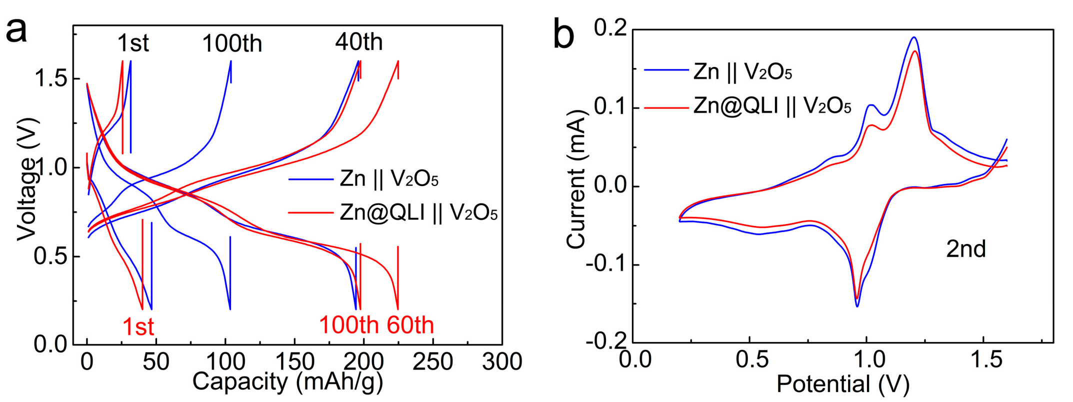

Figure S25. The galvanostatic voltage profiles (a) and CV curves (b) of the full cells.

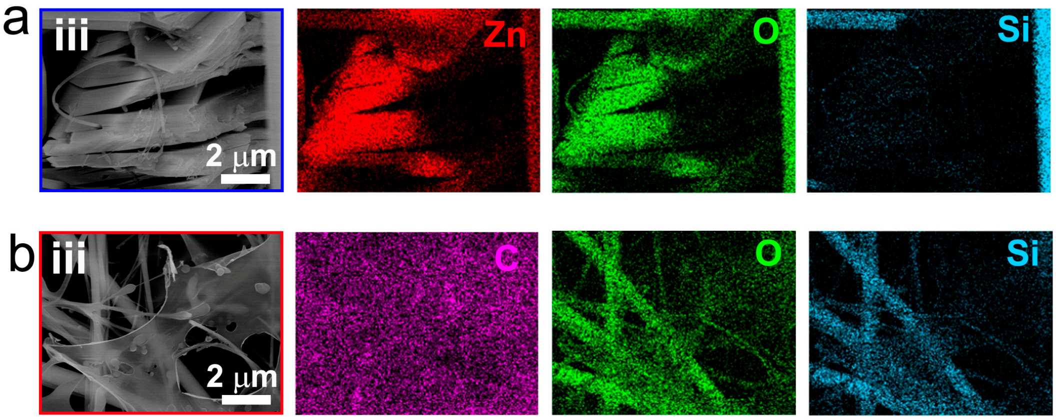

Figure S26. EDS mappings of the Zn (d) and Zn@QLI anode (e) after 300 cycles.

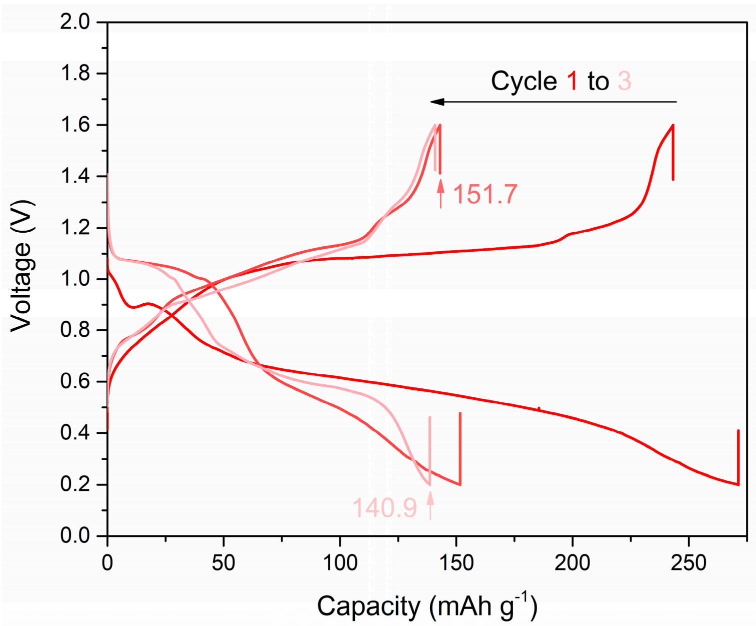

Figure S27. The galvanostatic voltage profiles of Zn@QLI-V_2O_5 full cell. The current 1 is 5 μA for cycle, and 10 μA for cycle 2-3. The cell was rest for 3 days after cycle 2, then conducted cycle 3 to test the self-discharge performance.

References

1. Chen, C.-H.; Pao, C.-W. Phase-field study of dendritic morphology in lithium metal batteries. *J. Power Sources* **2021**, *484*, 229203.

2. Liu, K.; Pei, A.; Lee, H. R.; Kong, B.; Liu, N.; Lin, D.; Liu, Y.; Liu, C.; Hsu, P. C.; Bao, Z.; et al. Lithium Metal Anodes with an Adaptive "Solid-Liquid" Interfacial Protective Layer. *J. Am. Chem. Soc.* **2017**, *139* (13), 4815-4820.

3. Wang, X.; Ao, Q.; Tian, X.; Fan, J.; Tong, H.; Hou, W.; Bai, S. Gelatin-Based Hydrogels for Organ 3D Bioprinting. *Polymers (Basel)* **2017**, *9* (9), 401.